ORIGINAL ARTICLE

Comparing the effects of uncoated nanostructured surfaces on primary neurons and astrocytes

Hanna Liliom[1] | Panna Lajer[1] | Zsófia Bérces[2,3] | Bence Csernyus[2] |

Ágnes Szabó[4] | Domonkos Pinke[5] | Péter Lőw[6] | Zoltán Fekete[4] |

Anita Pongrácz[3,4] | Katalin Schlett[1]

[1]Neuronal Cell Biology Research Group, Department of Physiology and Neurobiology, Institute of Biology, Eötvös Loránd University, Budapest, Hungary

[2]Faculty of Information Technology & Bionics, Pázmány Péter Catholic University, Budapest, Hungary

[3]Institute of Technical Physics and Materials Science, Centre for Energy Research, Hungarian Academy of Sciences, Budapest, Hungary

[4]Research Group for Implantable Microsystems, Faculty of Information Technology & Bionics, Pázmány Péter Catholic University, Budapest, Hungary

[5]Lab. of 3D Functional Network and Dendritic Imaging, Institute of Experimental Medicine, Hungarian Academy of Sciences, Budapest, Hungary

[6]Department of Anatomy, Cell and Developmental Biology, Institute of Biology, Eötvös Loránd University, Budapest, Hungary

Correspondence
Katalin Schlett, Department of Physiology and Neurobiology, Institute of Biology, Eötvös Loránd University, Pázmány Péter stny. 1/C, 1117 Budapest, Hungary.
Email: schlett.katalin@ttk.elte.hu

Abstract

The long-term application of central nervous system implants is currently limited by the negative response of the brain tissue, affecting both the performance of the device and the survival of nearby cells. Topographical modification of implant surfaces mimicking the structure and dimensions of the extracellular matrix may provide a solution to this negative tissue response and has been shown to affect the attachment and behavior of both neurons and astrocytes. In our study, commonly used neural implant materials, silicon, and platinum were tested with or without nanoscale surface modifications. No biological coatings were used in order to only examine the effect of the nanostructuring. We seeded primary mouse astrocytes and hippocampal neurons onto four different surfaces: flat polysilicon, nanostructured polysilicon, and platinum-coated versions of these surfaces. Fluorescent wide-field, confocal, and scanning electron microscopy were used to characterize the attachment, spreading and proliferation of these cell types. In case of astrocytes, we found that both cell number and average cell spreading was significantly larger on platinum, compared to silicon surfaces, while silicon surfaces impeded glial proliferation. Nanostructuring did not have a significant effect on either parameter in astrocytes but influenced the orientation of actin filaments and glial fibrillary acidic protein fibers. Neuronal soma attachment was impaired on metal surfaces while nanostructuring seemed to influence neuronal growth cone morphology, regardless of surface material. Taken together, the type of metals tested had a profound influence on cellular responses, which was only slightly modified by nanopatterning.

1 | INTRODUCTION

A great deal of research has been performed on central nervous system (CNS) implants to help patients suffering from diseases such as amyotrophic lateral sclerosis (ALS), spinal cord injury or paralysis. Effective long-term usage of such devices is limited by the defensive reaction of the CNS resulting in neuronal loss and glial scar formation. These events lead to the signal obstruction between neurons and electrodes during long-term implantation, degrade the performance of the neural electrodes causing instability, and eventually, the failure of the implanted device. The main aims of implant development are to improve neuronal survival and unimpeded regeneration and extension of neurites, while preventing microglial and astrocyte activation by keeping them from attaching to the implanted surface [see (Adewole, Serruya, Wolf, & Cullen, 2019; Fernandez & Botella, 2018; Jorfi, Skousen, Weder, & Capadona, 2015; Kim et al., 2018) for review].

One of the recent strategies is the topographical modification of neural implant surfaces, as imitating the structure of the extracellular matrix (ECM) can influence the attachment and behavior of neural cells (Jeon, Simon Jr, & Kim, 2014; Kim et al., 2018). The micro–/nanostructure of the implant surface can have a selective effect on astrocytes and neurons, demonstrated previously both in vitro and in vivo (Berces et al., 2016; Moxon et al., 2004; Moxon, Hallman, Aslani, Kalkhoran, & Lelkes, 2007; Piret, Perez, & Prinz, 2015). Proposed explanations by which nanostructuring results in better biocompatibility include the formation of mechanical cues similar to the ECM, and/or the adsorption of growth factors and other molecules facilitating the survival of neurons. However, the exact mechanisms involved are not yet clear (Marcus et al., 2017).

Many of the commercially available neural implants use silicon as a carrier material and platinum for the electrodes (Kotov et al., 2009). Platinum and silicon have been extensively characterized both in vivo and in vitro for their biocompatibility with neuronal cells and tissue (Biran, Martin, & Tresco, 2007; Ereifej et al., 2011; Griffith & Humphrey, 2006; Mols, Musa, Nuttin, Lagae, & Bonin, 2017; Pennisi et al., 2009; Polikov, Tresco, & Reichert, 2005). A wide variety of nanostructure types and sizes of these materials has been created and tested so far (Jeon et al., 2014; Kim et al., 2018; Kotov et al., 2009; Marcus et al., 2017), often in combination with the application of different ECM-like surface coatings (von der Mark, Park, Bauer, & Schmuki, 2010). On the other hand, the exact modifications of the nanopatterned surfaces generated by biomimetic coatings are hard to describe which further complicates the interpretation of the experimental findings (Kim et al., 2018).

Previously, our group has established the fabrication of so-called black polysilicon (Fekete, Horvath, Berces, & Pongracz, 2014), referred to as nanostructured silicon in this article. Such surfaces were created by large-area, maskless, and cryogenic plasma etching. This technology could be integrated easily into the manufacturing steps of silicon-based multichannel neural microelectrodes (Fekete, 2015). Earlier, we demonstrated that neuronal survival was increased in the vicinity of an uncoated black polysilicon implant surface 8 weeks after implantation, while the rate of glial activation was unaffected by nanostructuring (Berces et al., 2016).

In an attempt to more closely examine the initial cellular reactions behind these effects, we investigated the attachment and growth of primary mouse astroglial cells and hippocampal neurons on these metal surfaces, until a confluent cellular layer was formed. Tested materials included vapor deposited polycrystalline silicon (referred to as the "flat" surface) and its nanostructured counterpart created by photolithography, as well as the platinum sputter-coated version of both of these surfaces. As we wished to investigate the initial effects of cell-surface contact, cell behavior was analyzed during the first 3 days in culture. In order to more directly compare our in vitro and in vivo results, no additional surface coating to facilitate cell attachment was applied.

We found that nanostructuring in itself did not have a marked effect on the attachment, spreading and proliferation of astrocytes, while neuronal growth cones seemed to differentiate between flat and nanostructured surfaces. On the other hand, the attachment of neuronal soma was highly impaired on both metal surfaces.

2 | MATERIALS AND METHODS

2.1 | Design and manufacture of the in vitro test chips

Test chips for in vitro cell culturing were fabricated by standard MEMS processes in a way to contain all four different surfaces. In our study, flat polysilicon formed by low-pressure chemical vapor deposition or nanostructured polysilicon produced by cryogenic dry etching were used as seed layers and platinum deposited by DC magnetron sputtering was applied as coating material. To make well-defined interfaces between all four materials, we employed a specific chip design shown in Figure 1b. The manufacturing process is described in detail in an earlier publication by our group (Berces et al., 2018).

The four different experimental surfaces—flat polysilicon, nanostructured polysilicon, flat platinum, nanostructured platinum—were characterized by scanning electron microscopy (Figure 1a). In case of the nanostructured silicon surfaces, the height of the nanopillars was between 520 and 800 nm and pillar density was 18–70 pillars/μm^2, with pillar diameters of 80–150 nm. Flat polycrystalline silicon surfaces had a grain size of 100–200 nm. Both platinum surfaces possessed an additional thickness of 30 nm compared to the silicon surfaces. Chips were designed so that both large continuous regions as well as small rectangular geometries were created on each surface (Figure 1b).
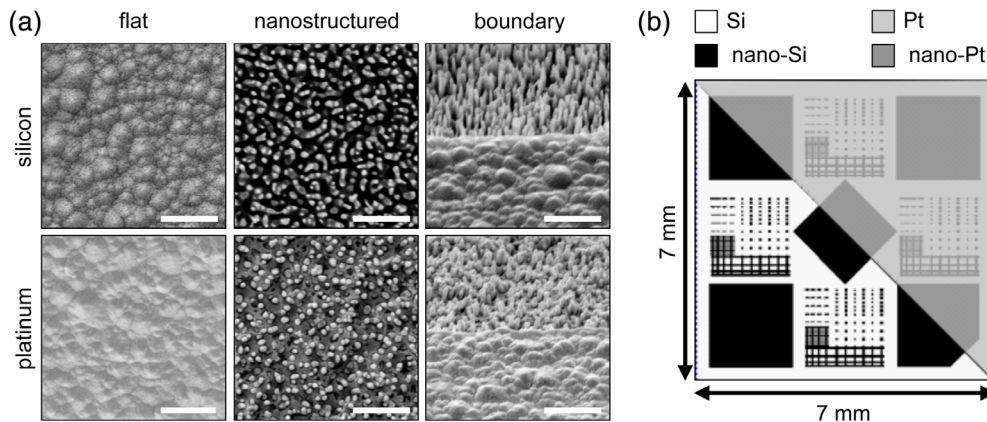
FIGURE 1   Surface and layout of the test chips. (a) Representative images of each experimental surface and the borders between the respective surfaces. Bars denote 1 μm. Left and central panels show surfaces viewed from the top; right panels are shown at a 45.5° angle. (b) Schematic of a single chip used in the study. White surfaces denote flat silicon (Si), black surfaces designate nanostructured silicon (nano-Si). Chips were coated diagonally with platinum, resulting in flat platinum (Pt; light gray) and nanostructured platinum (nano-Pt; dark gray)

2.2 | Animal handling

Wild-type CD1 mice were obtained from Charles River Laboratories (Wilmington, Massachusetts) and housed at $22 \pm 1°C$ with 12-hr light/dark cycles and ad libitum access to food and water. All experiments complied with local guidelines and regulations for the use of experimental animals (PEI/001/1108–4/2013 and PEI/001/1109–4/2013), in agreement with local and EU legislation.

2.3 | Primary cell cultures

Primary astrocytes were prepared postnatally from 1 to 4 days old mouse pups essentially according to a previously described method (Tarnok et al., 2010). Cultures were maintained in HDMEM (Sigma) with 10% FCS (Gibco), 2 mM glutamine (Sigma), 40 μg/mL gentamicin (Hungaropharma, Budapest, Hungary) and 2.5 μg/mL amphotericin B (Sigma). Cells were allowed to proliferate and passaged at least twice with 0.05% trypsin – 0.02% EDTA (Sigma) before being seeded onto test chips. Test chips were dry-heat sterilized at 180°C for 4 hr then placed in 24-well culture plates without any further surface treatment. Astrocytes were seeded at starting densities of 2.6×10^4 cells/cm².

Primary hippocampal neuronal cultures were prepared from 18-day-old mouse embryos, as previously described (Czondor et al., 2009). Neurons were seeded onto the test chips at densities of 6×10^4 cells/cm² and were maintained in Neurobasal medium (Life Technologies) supplemented with B27 (Life Technologies), 5% FCS, 0,5 mM glutamax (Invitrogen), 40 μg/mL gentamicin, and 2,5 μg/mL amphotericin B. All cultures were kept at 37°C in a 5% CO₂ atmosphere. Cells were fixed after 24, 48 or 72 hr.

2.4 | Immunocytochemistry, microscopy, and image processing

Cells were fixed with 4% paraformaldehyde (TAAB), permeabilized with 0.1% Triton-x-100 in phosphate buffered saline (PBS) and blocked using 2% bovine serum albumin (Sigma) in PBS solution. Neurons were immunostained with primary antibody anti-IIIβ-tubulin (1:1000, mouse, Exbio), while astrocytes were immunostained with anti-glial fibrillary acidic protein (GFAP) (1:1000, mouse, Sigma). The secondary antibody was anti-mouse-Alexa488 (1:500, Molecular Probes) in both cases. Staining with Alexa546-conjugated phalloidin (1:300, Molecular Probes) was used to visualize the actin cytoskeleton and DAPI was employed to visualize nuclei. Samples were mounted using Mowiol 4.88 (Polysciences, Hamburg, Germany).

Samples were investigated by a Zeiss Axio Observer Z1 or LSM800 inverted fluorescence microscope. Images were captured by an AxioCamMR3 camera or GasP detectors using ZEN software. Whole-chip scans were acquired by a mosaic-type image stitching technique using individual images of 10× magnification (obtained with a Plan-Neofluar 10×/0.30 objective). Individual images were captured by a Plan-Apochromat 63x/1.4 oil immersion objective and deconvoluted by the nearest neighbors method before z-projection.

To manually analyze the density of DAPI-stained astrocyte nuclei, the Cell Counter plugin of FIJI (Schindelin et al., 2012) was used. Average area covered by astrocytes or the average area of growth cone actin structures were also determined using FIJI, based on binarized images of phalloidin staining. To calculate the average area of individual cells within a 0.17 mm² ROI, the area covered by cells was divided by the total number of nuclei.

For automatized evaluation of the images, we used the Image Processing Toolbox of Matlab R2017b. Detailed description of the programming of our self-developed program, CellAnalyser, can be found in the Supplementary Information. Mean intensity and area values of the detected cell nuclei were calculated after background correction and cumulative histograms were created for every surface type.

2.5 | Scanning electron microscopy

Cells were fixed with 2.5% glutaraldehyde (Sigma) + 5% saccharose in 0.1 M cacodylate buffer for 1 hr at RT and dehydrated using increasing

concentrations of ethanol (50, 60, 75, 90, and 100%), and amyl-acetate (Sigma). Dried samples were sputter coated with gold for scanning electron microscopy. Samples were imaged using a LEO XB1540 (Zeiss) scanning electron microscope. Tilt angles are stated in figure legends. Surface characterization was performed using the ImageJ software.

2.6 | Statistics

The numbers of independent samples tested and the numbers of data points per experiment are noted in the legends of Figures 2 and 6. Statistical analyses for the results shown in Figure 2 were performed with SPSS Statistics (IBM). Normal distribution of the samples was evaluated using the Shapiro–Wilk test. Data was analyzed using one-way ANOVA

tests with post hoc Bonferroni corrections or the nonparametric Kruskal–Wallis test with pairwise comparisons. A p-value equal to or lower than .05 was considered as a statistically significant difference.

3 | RESULTS

3.1 | Attachment and spreading of primary astrocytes on uncoated silicon and platinum surfaces

We systematically analyzed the behavior of primary astrocytes seeded onto different test surfaces made from flat polysilicon, nanostructured polysilicon, flat platinum or nanostructured platinum before seeded cells reached confluency.
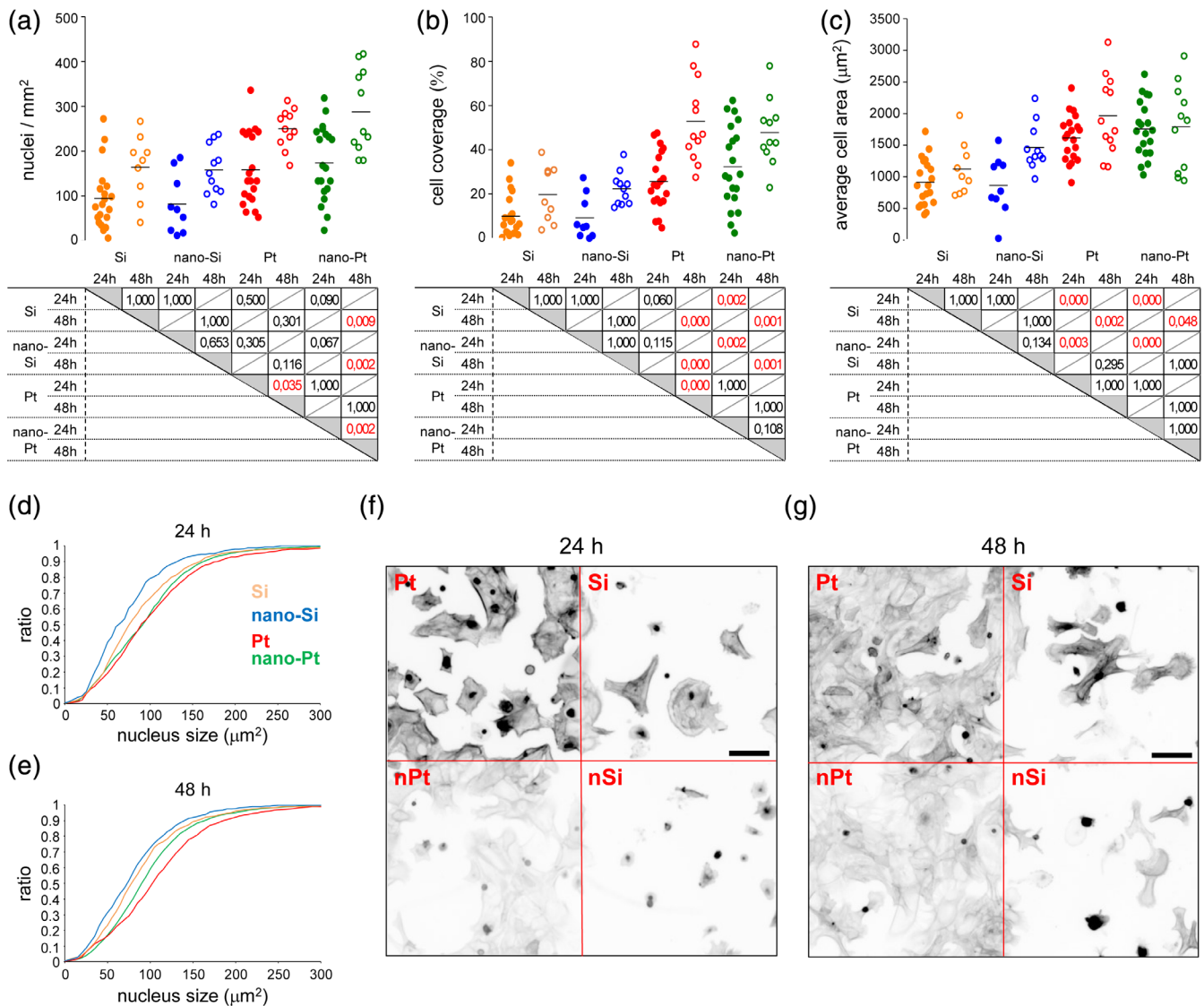

Table (a) — nuclei / mm²

	Si 24h	Si 48h	nano-Si 24h	nano-Si 48h	Pt 24h	Pt 48h	nano-Pt 24h	nano-Pt 48h
Si 24h		1,000	1,000		0,500		0,090	
Si 48h				1,000		0,301		0,009
nano-Si 24h				0,653	0,305		0,067	
nano-Si 48h						0,116		0,002
Pt 24h						0,035	1,000	
Pt 48h								1,000
nano-Pt 24h								0,002
nano-Pt 48h								

Table (b) — cell coverage (%)

	Si 24h	Si 48h	nano-Si 24h	nano-Si 48h	Pt 24h	Pt 48h	nano-Pt 24h	nano-Pt 48h
Si 24h		1,000	1,000		0,060		0,002	
Si 48h				1,000		0,000		0,001
nano-Si 24h				1,000	0,115		0,002	
nano-Si 48h						0,000		0,001
Pt 24h						0,000	1,000	
Pt 48h								1,000
nano-Pt 24h								0,108
nano-Pt 48h								

Table (c) — average cell area (μm²)

	Si 24h	Si 48h	nano-Si 24h	nano-Si 48h	Pt 24h	Pt 48h	nano-Pt 24h	nano-Pt 48h
Si 24h		1,000	1,000		0,000		0,000	
Si 48h				1,000		0,002		0,048
nano-Si 24h				0,134	0,003		0,000	
nano-Si 48h						0,295		1,000
Pt 24h						1,000	1,000	
Pt 48h								1,000
nano-Pt 24h								1,000
nano-Pt 48h								

FIGURE 2 Analysis of the total number (a), total surface area (b), average cell area (c) and nucleus size distribution (d–e) of astrocytes on the flat polysilicon [Si], nanostructured polysilicon [nano-Si], flat platinum [Pt] and nanostructured platinum [nano-Pt]. (a–c) Data points show values for the individual ROIs. Horizontal line through data points shows median value. Exact p values are shown in the tables below the graphs, with $p < .05$ in red. (d, e) Cumulative histograms of nucleus size (d) 24 or (e) 48 hr post-seeding. All data were obtained from 3 to 4 independently seeded test chips. Data points per experiment varied between 9 and 20. (f, g) Representative images of primary astrocyte cultures used for quantitative analysis fixed at either (f) 24 or (g) 48 hr post seeding. Inverted images of fluorescent phalloidin staining reveal the actin cytoskeleton of astrocytes over adjacent surfaces. Scale bars denote 100 μm

Cell density was calculated upon staining the nuclei with DAPI. By 24 hr after seeding, a similar cell density was found on each surface, indicating that neither the surface material nor nanostructuring had an effect on the initial attachment of astrocytes (Figure 2a). When analyzing the changes in cell densities on the same surface 24 hr later, we found that average number of nuclei increased significantly only on platinum surfaces. This implies that astrocyte proliferation is impeded on silicon, regardless of surface architecture. The effect of nanostructuring itself was revealed only in case of nanostructured platinum, as at 48 hr, significantly more cells were present on this surface compared to silicon.

The degree of astrocyte spreading on the different surfaces was determined by phalloidin staining of the actin cytoskeleton (Figure 2b, for representative images, see Figure 2f,g). When we compared the area covered by astrocytes 24 hr after seeding, we found that the degree of cell coverage was significantly higher on nanostructured platinum compared to silicon. In the next 24 hr, cell coverage increased significantly only on flat platinum. As a consequence, both platinum surfaces differed significantly compared to flat and nanostructured silicon 48 hr after seeding. By the third day after seeding, cultures seeded onto platinum surfaces reached confluency (data not shown).

In order to compare the average extent of cell spreading, average cell area values were calculated by dividing the area of cell covered surface by the corresponding number of DAPI-stained nuclei within the individual ROIs (Figure 2c). 24 hr post-seeding, astrocytes were less spread over silicon compared to cells on either flat or nanostructured platinum. Interestingly, this difference was only observed between flat silicon and the two platinum surfaces at 48 hr post-seeding. At this time, average cell area values on nanostructured silicon showed a slight increase compared to the values for flat silicon, but no significant change was determined compared to any of the other surface type. Average astrocyte surface area remained similar between 24 and 48 hr after seeding, indicating that cell proliferation did not influence cell spreading.

We also evaluated the distribution of nucleus size on the different surfaces with a custom-made algorithm (see Supplementary Information for a detailed description) and visualized the data using cumulative histograms (Figure 2d,e). According to this analysis, 24 hr after seeding astrocytes had the smallest nuclei on nanostructured silicon, followed by the flat silicon surface. The size distribution of nuclei was very similar in case of flat and nanostructured platinum (Figure 2d). 48 hr after seeding, no marked difference was found between both silicon surface and nanostructured platinum. However, nuclei were larger over flat platinum (Figure 2e).

To assist in the direct comparison of the effect induced by different surface types, representative chip areas incorporating both flat and nanostructured silicon and platinum are shown 24 (Figure 2f) or 48 hr (Figure 2g) after seeding. Astrocytes were visualized by phalloidin staining of the actin system. In agreement with our quantitative measurements, astrocytes spread more on platinum and achieved significantly higher confluence by 48 hr compared to the

silicon surfaces. It is also evident from the images that astrocytes were generally smaller on silicon (Figure 2f,g).

Using widefield fluorescent microscopy, a notable difference in phalloidin (Figure 2f,g) fluorescent signal intensity over flat or nanostructured surfaces was evident. These differences are mainly due to the increased light absorbance of the nonreflecting nanostructured surfaces (Fekete et al., 2014). On the other hand, astroglial cells showed stronger fluorescence over silicon surfaces comparing to the same type of platina surfaces, especially 48 hr after seeding.

Examination of individual astrocytes by confocal microscopy revealed further differences between the test surfaces (Figure 3). A general observation in case of platinum surfaces was that filamentous actin in astrocytes was present in bundles indicative of well-developed stress fibers. In contrast, astrocytes attached to silicon had shorter and thinner actin fibers, which, especially in case of the nanostructured silicon, were often arranged in a radial pattern. GFAP intermedier filaments were more linear and mostly radially oriented in cells attached to either nanostructured surface. On the other hand, astrocytes grown over flat surfaces had thicker and more focally organized GFAP filaments.

In addition to fluorescent light microscopy, we also employed scanning electron microscopy (SEM) to examine astrocyte attachment to the different surface types. SEM images revealed that in case a cell attached to the test chip in the vicinity of or across a flat-nanostructured surface boundary, glial protrusions often seemed to avoid (Figure 4a,b) or detach from (Figure 4c,d) nanostructured surfaces.

3.2 | Attachment and spreading of primary hippocampal neurons on uncoated silicon and platinum surfaces

In order to test the attachment of neurons to the different surfaces, primary neuronal cultures dissociated from the hippocampi of 18-day-old mouse embryos were seeded onto the test chips. At this age of isolation, most of the isolated cells are neurons while astroglial cells form less than 5% of the cell suspension [data not shown]. In contrast to astroglial cells, primary hippocampal neurons attached very poorly to all of the uncoated metal surfaces. Instead, neuronal cell bodies attached to each other and formed aggregates with various sizes, containing either a few or up to several hundreds of cells. Surface-attached astroglial cells, on the other hand, provided an attractive substrate for aggregates as well as for outgrowing neurites (Figure 5). As expected, neurite extension on top of the attached astroglial cells was not affected by the baseline surface material nor nanostructuring (Figure 5).

Occasionally, neurites spread out to the noncovered uncoated metal surfaces, as well (Figure 6). Scanning electron microscopy revealed that growth cones attached to nanopatterned surfaces had narrow lamellopodia separated by several filopodia. In contrast, growth cones attached to flat surfaces did not possess distinct lamellopodia and often tapered to a point (Figure 6a).

FIGURE 3 Representative images of deconvoluted and z-projected confocal images of individual astrocytes. From left to right, columns show black-and-white inverted fluorescent signals denoting the actin cytoskeleton (phalloidin), glial fibrillary acidic protein (anti-GFAP) and the nucleus (DAPI). Right columns show the merged phalloidin (magenta) and anti-GFAP (green) signals. Scale bars denote 10 μm
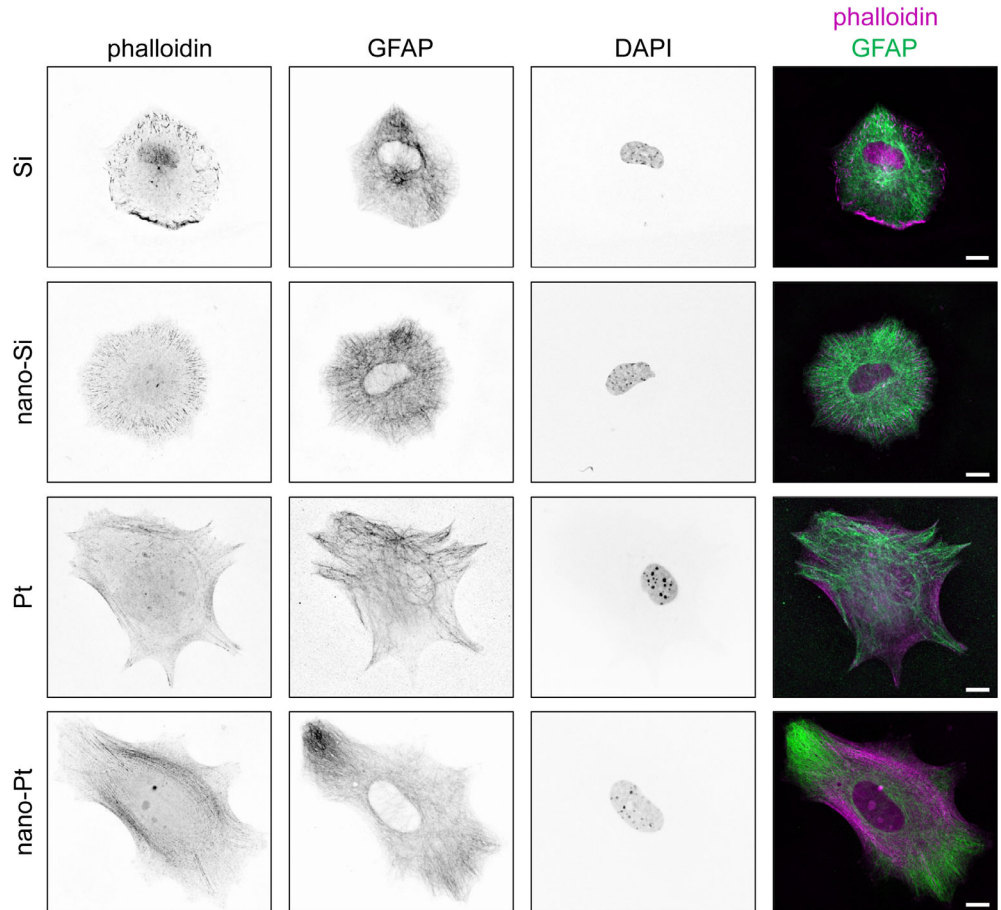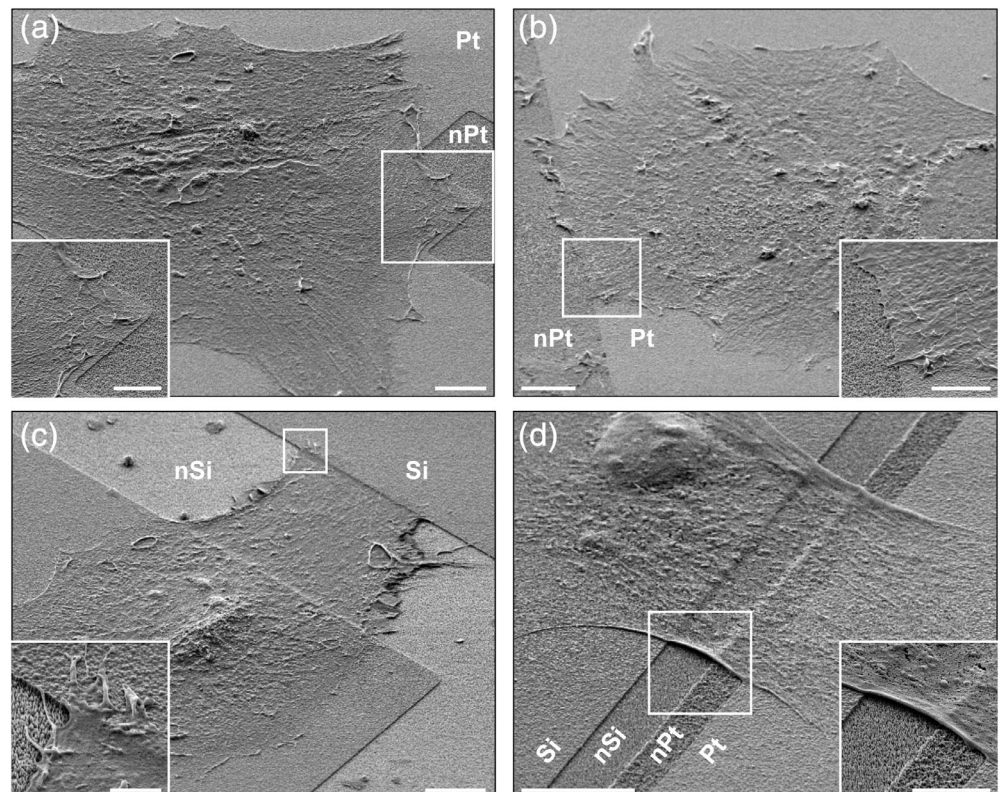

FIGURE 4 Scanning electron microscopy images of individual astrocytes attached across or near flat-nanostructured surface boundaries. The surface types—flat polysilicon, nanostructured polysilicon, flat platinum and nanostructured platinum—are marked as Si, nSi, Pt, and nPt, respectively. Enlarged image areas delineated by white squares are shown in the bottom left (a) or right (b–d) corners. Scale bars in full-sized images denote 10 μm, while bars in insets denote (a, b, d) 5 or (c) 2 μm
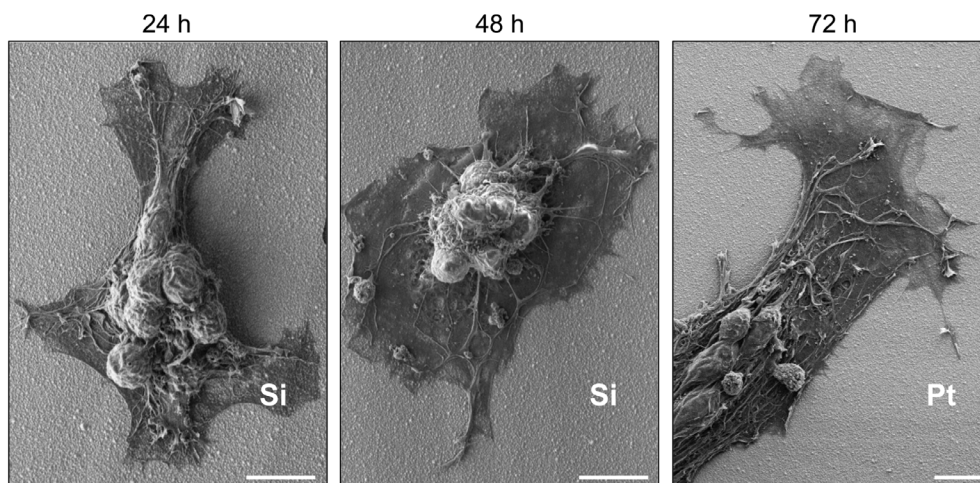
24 h	48 h	72 h

FIGURE 5 Scanning electron microscopy images of aggregated primary hippocampal neurons attached to primary astrocytes on flat polysilicon (Si) or platinum (Pt) surface 24, 48 or 72 hr post-seeding. Bars denote 10 μm

To examine the cytoskeleton of these growth cones, we performed immunostaining to detect neuron-specific IIIβ-tubulin and phalloidin staining to visualize filamentous actin. Microtubule localization was similar in all investigated growth cones, mainly forming bundles (Figure 6b). In agreement with growth cone topology, the actin cytoskeleton was arranged in a mesh-like pattern within the lamellopodia over nanostructured silicon and platinum. We also compared the extent of the actin network within the growth cones, by measuring the area of phalloidin staining over different surfaces (Figure 6c). Although only a few individual growth cones were found on each surface, there is a clear trend of more extensive actin structures on top of both nanostructured surface types.

In summary, these observations indicate that uncoated silicon and platinum surfaces do not promote the attachment of primary neuronal cell bodies. Nanostructuring of these surfaces, on the other hand, may selectively promote neurite outgrowth.

4 | DISCUSSION

Silicon and platinum have been characterized extensively in terms of biocompatibility for implantable device applications (Biran et al., 2007; Ereifej et al., 2011; Mols et al., 2017; Pennisi et al., 2009; Polikov et al., 2005), but fewer publications tested uncoated silicon or platinum surfaces.(Biran, Martin, & Tresco, 2005; Pennisi et al., 2009) As bare surfaces are less biocompatible, biomimetic coatings are often used to improve their performance (Adewole et al., 2019; Fernandez & Botella, 2018; Jorfi et al., 2015; Polikov et al., 2005). Part of previous research on the effect of nanostructuring on neural cells in vitro involved surfaces additionally treated with molecules such as poly-D-lysine/poly-L-lysine and laminin to aid cell adhesion and survival on otherwise biologically inert materials (Bugnicourt, Brocard, Nicolas, & Villard, 2014; Huang et al., 2018). Use of biomimetic coatings is also a promising strategy in itself for attenuating the negative tissue response to CNS implants (Aregueta-Robles, Woolley, Poole-Warren, Lovell, & Green, 2014; Jorfi et al., 2015), however, little is known about their persistence, longevity or adverse effects in an in vivo

setting (Adewole et al., 2019; Chen, Canales, & Anikeeva, 2017; Cody, Eles, Lagenaur, Kozai, & Cui, 2018; He, McConnell, & Bellamkonda, 2006; Rao & Winter, 2009). So far, only the lack of coating degradation in response to the insertion process was shown (He et al., 2006). Therefore, it is important to examine whether the modification of implant surface topography in itself is capable of significantly affecting neural cell behavior.

Consequently, we extended our previous in vivo and in vitro studies by testing chronic responses to similar implant surfaces within the brain (Berces et al., 2016) or acute effects on immortalized neural stem cells and microglia (Berces et al., 2018), respectively. We aimed to compare how primary astrocytes and hippocampal neurons attach to flat or nanostructured silicon or platinum surfaces without additional coating. Our primary goal was to examine the effect of these materials on the spreading and proliferation of astrocytes and on neurite outgrowth within the initial days after seeding, until glial cells reach confluency.

In our study, neither bare silicon or platinum induced an acute cytotoxic effect on neurons or astrocytes during the experimental period, in agreement with previous studies (Ereifej et al., 2011; Kang et al., 2016). In accordance with previous studies, we found that direct attachment of primary hippocampal neurons to both uncoated metal surfaces was impaired (Khan, Auner, & Newaz, 2005; Piret, Perez, & Prinz, 2014). Earlier in vitro studies involving primary neurons that did not utilize additional surface treatment showed similar clusters of neurons sitting on top of glial cells in case of both nonstructured (Piret et al., 2014) and nanostructured silicon surfaces (Khan et al., 2005). In other cases, the morphology of the examined cells was clearly not neuronal (Ma, Liu, Xu, & Cui, 2005). There are also reports where neurons were apparently able to directly attach to uncoated silicon surfaces, but some of these surfaces also had a cytotoxic effect after 5 days of culture (Fan et al., 2002; Fan et al., 2002) or the presence of surface coating was not clearly stated (Kang et al., 2016).

In case neurites did attach to the tested surfaces, growth cone formation appeared to be promoted by nanostructuring. Similarly, an increase in neurite outgrowth on nanostructured relative to smoother surfaces has been demonstrated in several studies (Bugnicourt et al.,
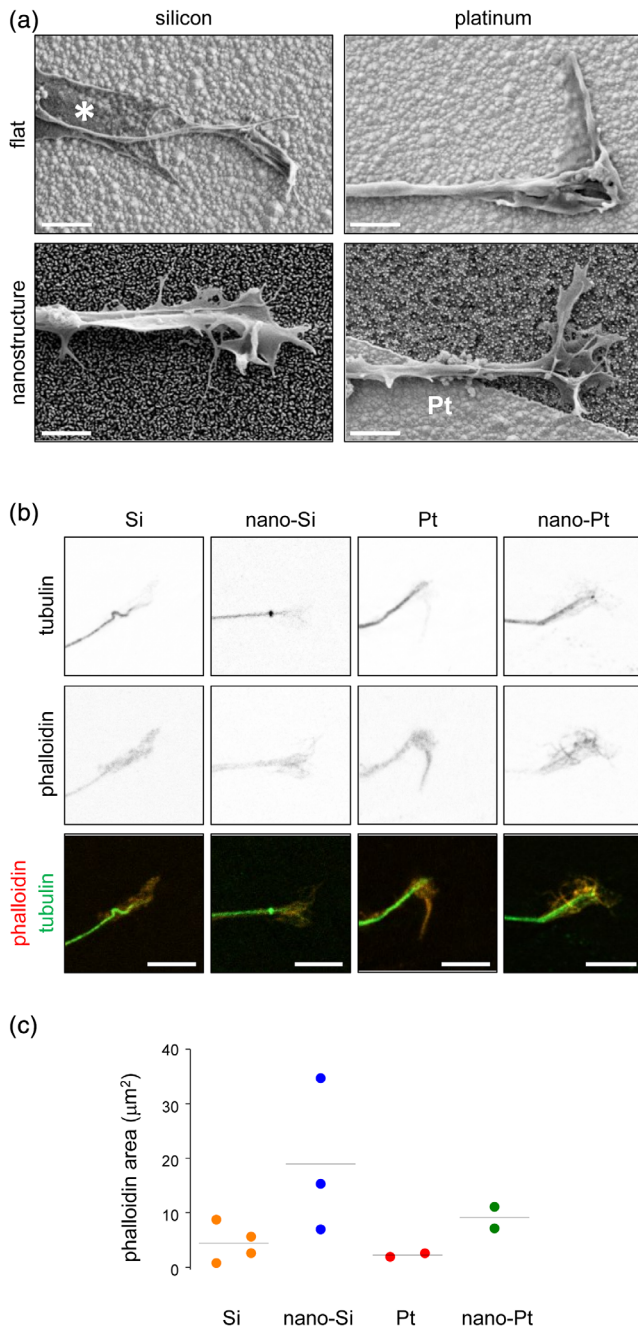
FIGURE 6 Representative images of neuronal growth cones directly attached to the different uncoated experimental surfaces.
(a) Representative images produced by scanning electron microscopy. Asterisk in the upper left image marks the edge of a glial process. Scale bars denote 2 μm. (b) Deconvoluted and z-projected confocal images of individual neuronal growth cones over flat polysilicon (Si), nanostructured polysilicon (nano-Si), flat platinum (Pt), and nanostructured platinum (nano-Pt). Upper and middle images display inverted fluorescent signals of neuron-specific IIIβ-tubulin or phalloidin. Bottom images show the merged phalloidin (red) and anti-tubulin (green) signals. Scale bars denote 5 μm. (c) Data points show the area of phalloidin staining within individual neuronal growth cones on flat polysilicon (Si), nanostructured polysilicon (nano-Si), flat platinum (Pt), and nanostructured platinum (nano-Pt). Horizontal line through data points shows median value. All data were obtained from four independently seeded test chips. Data points per experiment varied between 1 and 5

2014; Moxon et al., 2004; Moxon et al., 2007). Kang and colleagues also showed enhanced and more directed neurite extension on silicon nanowires, however, growth cones on top of the nanowires were narrower compared to those on flat silicon (Kang et al., 2016). It is important to note that the apparent differences compared to our results might be explained by different surface composition and/or coating between the studies.

Our results regarding the behavior of astrocytes are in agreement with another study focusing on the effects of uncoated, non-structured silicon and platinum surfaces on several aspects of glioblastoma behavior in vitro (Ereifej et al., 2011; Ereifej et al., 2013). In the report by Ereifej and colleagues, the observed effects of silicon and platinum were attributed to increased glial reactivity, which was not examined directly in our study. Due to differences in the reflectivity of the tested metal surfaces, we could not reliably compare the fluorescent intensity of anti-GFAP immunostaining as an indicator of astrocyte reactivity. However, our results showed increased proliferation as well as greater spreading of astrocytes grown on platinum, indicating that uncoated platinum provides a more suitable surface for primary astroglial cells than silicon. Nanostructuring itself did not affect cell spreading but cytoskeletal orientation was changed and resulted in thinner GFAP fibers, which were more radially oriented. Pennisi and colleagues also found that the morphology and proliferation of a glial cell line was not markedly affected on either of the examined nanostructures (Pennisi et al., 2009). In other studies, changes in gene expression point toward a reactivity reducing effect of nanostructured surfaces (Ereifej et al., 2013; Ereifej et al., 2018).

In line with the above results, previous work by our group (Berces et al., 2016) and others (Chapman et al., 2017; Moxon et al., 2007; Piret et al., 2014) reported that nanostructuring affects primary astrocytes/glial cell lines and primary neurons/neuronal cell lines in a different manner. in vivo results also demonstrated no effect of microstructuring on astrocyte reactivity while the number of surviving neurons was positively affected by the topographical modification (Moxon et al., 2007). Neuronal attachment was unaffected by nanoporous gold surfaces, while astrocytic coverage was decreased compared to a nonstructured surface of the same material (Chapman et al., 2017). Additionally, Piret and colleagues were able to separate primary neurons from glia with vertically grown nanowires, although a marked separation of the two cell types was only achieved in case of alternating large contiguous flat and nanostructured surfaces—narrower arrays or single rows of nanowires did not induce such an effect (Piret et al., 2015). Interestingly, we observed that astrocytes frequently aligned along surface boundaries between flat and nanostructured regions, which might be explained by a sensitivity to steep changes in surface architecture.

The surface modification of polysilicon thin films resulted in a silicon nanostructure with dimensions in the same range as the 150–200 nm diameter of typical collagen fibrils in the extracellular matrix (Garvin, VanderBurgh, Hocking, & Dalecki, 2013; Li, Zhu, Strakova, & Wang, 2014; Shoulders & Raines, 2009). Neurons have been shown to be sensitive to surface roughness on the scale of nanometers, and—in case of silicon-based structures—have been

reported to best attach to and survive on surfaces with average surface roughness (Ra) values ranging from 20 to 100 nm. Both lower and higher values were found to negatively affect cell adhesion and viability, albeit to a different degree in different studies (Fan, Cui, Chen, et al., 2002; Fan, Cui, Hou, et al., 2002; Ma et al., 2005). Other studies concluded that pillar height of nanostructures influences the cellular adhesion and viability and can determine whether cells spread on top of the nanostructures or grow into the trenches between them (Choi et al., 2007; Piret, Perez, & Prinz, 2013). It can be speculated that the feature size of our nanostructured surfaces inhibited the adhesion of the neuronal somas. On the other hand, implantable device performance does not necessarily depend on the attachment of the neuronal somas, however, the unimpeded—and possibly guided–growth of neurites along the implant surface would be crucial to improve long-term functioning.

It must be noted that it is difficult to directly compare results from different groups related to this aspect due to large variations in fabrication methods, applied surface treatments, cleaning protocols and the resulting features themselves in terms of shape, size, and distribution. The exact feature dimensions different research groups choose to publish are also not uniform [see (Marcus et al., 2017) for review]. Therefore, further investigation is needed in order to clarify the effects of nanostructured materials on neural cell types.

In conclusion, we detected that nanostructuring of artificial silicon and platinum surfaces without any biomimetic coating do not affect the attachment and morphology of astrocytes. The type of surface material, on the other hand, had profound influence on cellular responses, further emphasizing that metal implants are less suitable for potential in vivo usage compared to other more promising materials (Chen et al., 2017; Feiner & Dvir, 2018).

ACKNOWLEDGMENTS

ORCID

Katalin Schlett https://orcid.org/0000-0001-9265-4236

REFERENCES

Adewole, D. O., Serruya, M. D., Wolf, J. A., & Cullen, D. K. (2019). Bioactive Neuroelectronic Interfaces. *Frontiers in Neuroscience*, 13, 269.

Aregueta-Robles, U. A., Woolley, A. J., Poole-Warren, L. A., Lovell, N. H., & Green, R. A. (2014). Organic electrode coatings for next-generation neural interfaces. *Frontiers in neuroengineering*, 7, 15.

Berces, Z., Pomothy, J., Horvath, A. C., Kohidi, T., Benyei, E., Fekete, Z., ... Pongracz, A. (2018). Effect of nanostructures on anchoring stem cell-derived neural tissue to artificial surfaces. *Journal of Neural Engineering*, 15(5), 056030.

Berces, Z., Toth, K., Marton, G., Pal, I., Kovats-Megyesi, B., Fekete, Z., ... Pongracz, A. (2016). Neurobiochemical changes in the vicinity of a nanostructured neural implant. *Scientific Reports*, 6, 35944.

Biran, R., Martin, D. C., & Tresco, P. A. (2005). Neuronal cell loss accompanies the brain tissue response to chronically implanted silicon microelectrode arrays. *Experimental Neurology*, 195(1), 115–126.

Biran, R., Martin, D. C., & Tresco, P. A. (2007). The brain tissue response to implanted silicon microelectrode arrays is increased when the device is tethered to the skull. *Journal of Biomedical Materials Research Part A*, 82A(1), 169–178.

Bugnicourt, G., Brocard, J., Nicolas, A., & Villard, C. (2014). Nanoscale surface topography reshapes neuronal growth in culture. *Langmuir*, 30(15), 4441–4449.

Chapman, C. A. R., Wang, L., Chen, H., Garrison, J., Lein, P. J., & Seker, E. (2017). Nanoporous gold biointerfaces: Modifying nanostructure to control neural cell coverage and enhance electrophysiological recording performance. *Advanced Functional Materials*, 27(3), https://onlinelibrary.wiley.com/doi/full/10.1002/adfm.201604631.

Chen, R., Canales, A., & Anikeeva, P. (2017). Neural recording and modulation technologies. *Nature Reviews Materials*, 2(2), https://www.nature.com/articles/natrevmats201693.

Choi, C. H., Hagvall, S. H., Wu, B. M., Dunn, J. C., Beygui, R. E., & CJK, C. J. (2007). Cell interaction with three-dimensional sharp-tip nanotopography. *Biomaterials*, 28(9), 1672–1679.

Cody, P. A., Eles, J. R., Lagenaur, C. F., Kozai, T. D. Y., & Cui, X. T. (2018). Unique electrophysiological and impedance signatures between encapsulation types: An analysis of biological Utah array failure and benefit of a biomimetic coating in a rat model. *Biomaterials*, 161, 117–128.

Czondor, K., Ellwanger, K., Fuchs, Y. F., Lutz, S., Gulyas, M., Mansuy, I. M., ... Schlett, K. (2009). Protein kinase D controls the integrity of Golgi apparatus and the maintenance of dendritic arborization in hippocampal neurons. *Molecular Biology of the Cell*, 20(7), 2108–2120.

Ereifej, E. S., Khan, S., Newaz, G., Zhang, J. S., Auner, G. W., & VandeVord, P. J. (2011). Characterization of astrocyte reactivity and gene expression on biomaterials for neural electrodes. *Journal of Biomedical Materials Research Part A*, 99A(1), 141–150.

Ereifej, E. S., Matthew, H. W., Newaz, G., Mukhopadhyay, A., Auner, G., Salakhutdinov, I., & VandeVord, P. J. (2013). Nanopatterning effects on astrocyte reactivity. *Journal of Biomedical Materials Research Part A*, 101(6), 1743–1757.

Ereifej, E. S., Rial, G. M., Hermann, J. K., Smith, C. S., Meade, S. M., Rayyan, J. M., ... Capadona, J. R. (2018). Implantation of neural probes in the brain elicits oxidative stress. *Frontiers in Bioengineering and Biotechnology*, 6, 9.

Fan, Y. W., Cui, F. Z., Chen, L. N., Zhai, Y., Xu, Q. Y., & Lee, I. S. (2002). Adhesion of neural cells on silicon wafer with nano-topographic surface. *Applied Surface Science*, 187(3–4), 313–318.

Fan, Y. W., Cui, F. Z., Hou, S. P., Xu, Q. Y., Chen, L. N., & Lee, I. S. (2002). Culture of neural cells on silicon wafers with nano-scale surface topograph. *Journal of Neuroscience Methods*, 120(1), 17–23.

Feiner, R., & Dvir, T. (2018). Tissue-electronics interfaces: From implantable devices to engineered tissues. *Nature Reviews Materials*, 3(1), https://www.nature.com/articles/natrevmats201776.

Fekete, Z. (2015). Recent advances in silicon-based neural microelectrodes and microsystems: A review. *Sensors and Actuators B: Chemical*, 215, 300–315.

Fekete, Z., Horvath, A. C., Berces, Z., & Pongracz, A. (2014). Black poly-silicon: A nanostructured seed layer for sensor applications. *Sensors and Actuators A: Physical*, 216, 277–286.

Fernandez, E., & Botella, P. (2018). Biotolerability of Intracortical microelectrodes. *Advanced Biosystems*, 2(1), https://doi.org/10.1002/adbi.201700115.

Garvin, K. A., VanderBurgh, J., Hocking, D. C., & Dalecki, D. (2013). Controlling collagen fiber microstructure in three-dimensional hydrogels using ultrasound. *The Journal of the Acoustical Society of America*, 134 (2), 1491–1502.

Griffith, R. W., & Humphrey, D. R. (2006). Long-term gliosis around chronically implanted platinum electrodes in the rhesus macaque motor cortex. *Neuroscience Letters*, 406(1–2), 81–86.

He, W., McConnell, G. C., & Bellamkonda, R. V. (2006). Nanoscale laminin coating modulates cortical scarring response around implanted silicon microelectrode arrays. *Journal of Neural Engineering*, 3(4), 316–326.

Huang, Y. M., Jiang, Y., Wu, Q. Y., Wu, X. B., An, X. D., Chubykin, A. A., … Yang, C. (2018). Nanoladders facilitate directional axonal outgrowth and regeneration. *ACS Biomaterials Science & Engineering*, 4(3), 1037–1045.

Jeon, H., Simon, C. G., Jr., & Kim, G. (2014). A mini-review: Cell response to microscale, nanoscale, and hierarchical patterning of surface structure. *Journal of Biomedical Materials Research Part B: Applied Biomaterials*, 102(7), 1580–1594.

Jorfi, M., Skousen, J. L., Weder, C., & Capadona, J. R. (2015). Progress towards biocompatible intracortical microelectrodes for neural interfacing applications. *Journal of Neural Engineering*, 12(1), 011001.

Kang, K., Park, Y. S., Park, M., Jang, M. J., Kim, S. M., Lee, J., … Choi, I. S. (2016). Axon-first Neuritogenesis on vertical nanowires. *Nano Letters*, 16(1), 675–680.

Khan, S. P., Auner, G. G., & Newaz, G. M. (2005). Influence of nanoscale surface roughness on neural cell attachment on silicon. *Nanomedicine: Nanotechnology Biology and Medicine*, 1(2), 125–129.

Kim, Y., Meade, S. M., Chen, K., Feng, H., Rayyan, J., Hess-Dunning, A., & Ereifej, E. S. (2018). Nano-architectural approaches for improved intracortical interface technologies. *Frontiers in Neuroscience*, 12, 456.

Kotov, N. A., Winter, J. O., Clements, I. P., Jan, E., Timko, B. P., Campidelli, S., … Ballerini, L. (2009). Nanomaterials for neural interfaces. *Advanced Materials*, 21(40), 3970–4004.

Li, W., Zhu, B., Strakova, Z., & Wang, R. (2014). Two-way regulation between cells and aligned collagen fibrils: Local 3D matrix formation and accelerated neural differentiation of human decidua parietalis placental stem cells. *Biochemical and Biophysical Research Communications*, 450(4), 1377–1382.

Ma, J., Liu, B. F., Xu, Q. Y., & Cui, F. Z. (2005). AFM study of hippocampal cells cultured on silicon wafers with nano-scale surface topograph. *Colloids and Surfaces B: Biointerfaces*, 44(2–3), 152–157.

Marcus, M., Baranes, K., Park, M., Choi, I. S., Kang, K., & Shefi, O. (2017). Interactions of neurons with physical environments. *Advanced Healthcare Materials*, 6(15), https://onlinelibrary.wiley.com/doi/full/10.1002/adhm.201700267.

Mols, K., Musa, S., Nuttin, B., Lagae, L., & Bonin, V. (2017). In vivo characterization of the electrophysiological and astrocytic responses to a silicon neuroprobe implanted in the mouse neocortex. *Scientific Reports*, 7, 15642.

Moxon, K. A., Hallman, S., Aslani, A., Kalkhoran, N. M., & Lelkes, P. I. (2007). Bioactive properties of nanostructured porous silicon for enhancing electrode to neuron interfaces. *Journal of Biomaterials Science. Polymer Edition*, 18(10), 1263–1281.

Moxon, K. A., Kalkhoran, N. M., Markert, M., Sambito, M. A., McKenzie, J. L., & Webster, J. T. (2004). Nanostructured surface modification of ceramic-based microelectrodes to enhance biocompatibility for a direct brain-machine interface. *IEEE Transactions on Biomedical Engineering*, 51(6), 881–889.

Pennisi, C. P., Sevcencu, C., Dolatshahi-Pirouz, A., Foss, M., Hansen, J. L., Larsen, A. N., … Yoshida, K. (2009). Responses of fibroblasts and glial cells to nanostructured platinum surfaces. *Nanotechnology*, 20(38), 385103.

Piret, G., Perez, M. T., & Prinz, C. N. (2013). Neurite outgrowth and synaptophysin expression of postnatal CNS neurons on GaP nanowire arrays in long-term retinal cell culture. *Biomaterials*, 34(4), 875–887.

Piret, G., Perez, M. T., & Prinz, C. N. (2014). Substrate porosity induces phenotypic alterations in retinal cells cultured on silicon nanowires. *RSC Advances*, 4(53), 27888–27897.

Piret, G., Perez, M. T., & Prinz, C. N. (2015). Support of neuronal growth over glial growth and guidance of optic nerve axons by vertical nanowire arrays. *ACS Applied Materials & Interfaces*, 7(34), 18944–18948.

Polikov, V. S., Tresco, P. A., & Reichert, W. M. (2005). Response of brain tissue to chronically implanted neural electrodes. *Journal of Neuroscience Methods*, 148(1), 1–18.

Rao, S. S., & Winter, J. O. (2009). Adhesion molecule-modified biomaterials for neural tissue engineering. *Frontiers in neuroengineering*, 2, 6.

Schindelin, J., Arganda-Carreras, I., Frise, E., Kaynig, V., Longair, M., Pietzsch, T., … Cardona, A. (2012). Fiji: An open-source platform for biological-image analysis. *Nature Methods*, 9(7), 676–682.

Shoulders, M. D., & Raines, R. T. (2009). Collagen structure and stability. *Annual Review of Biochemistry*, 78, 929–958.

Tarnok, K., Szilagyi, L., Berki, T., Nemeth, P., Graf, L., & Schlett, K. (2010). Anoxia leads to a rapid translocation of human trypsinogen 4 to the plasma membrane of cultured astrocytes. *Journal of Neurochemistry*, 115(2), 314–324.

von der Mark, K., Park, J., Bauer, S., & Schmuki, P. (2010). Nanoscale engineering of biomimetic surfaces: Cues from the extracellular matrix. *Cell and Tissue Research*, 339(1), 131–153.

SUPPORTING INFORMATION

Additional supporting information may be found online in the Supporting Information section at the end of this article.